State Dependent Multiple Model-Based Particle Filtering for Ballistic Missile Tracking in a Low-Observable Environment

Miao Yu[a], Wen-Hua Chen[a], Jonathon Chambers[b]

[a] *Department of Aeronautical and Automotive Engineering, Loughborough University, LE11 3TU, UK*
[b] *School of Electrical and Electronic Engineering, Newcastle University, NE1 7RU, UK*

Abstract

This paper proposes a new method for tracking the whole trajectory of a ballistic missile (BM), in a low-observable environment with 'imperfect' sensor measurement incorporating both miss detection and false alarms. A hybrid system with state dependent transition probabilities is proposed where multiple state models represent the ballistic missile movement during different phases; and domain knowledge is exploited to model the transition probabilities between different flight phases in a state-dependent way. The random finite set (RFS) is adopted to model radar sensor measurements which include both miss detection and false alarms. Based on the proposed hybrid modeling system and the RFS represented sensor measurements, a state dependent interacting multiple model particle filtering method integrated with a generalized measurement likelihood function is developed for the BM tracking. Comprehensive simulation studies show that the proposed method outperforms the traditional ones for the BM tracking, with more accurate estimations of flight mode probabilities, positions and velocities.

Keywords: multiple model, state dependent, random finite set, miss detection, false alarm, particle filter

1. Introduction

A ballistic missile (BM) is one of the major threats from the air, which poses threats to civilians, territory and deployed forces. Missile defense systems have been built to intercept a hostile BM(s) before hitting a target in modern warfare. For the BM interception, one essential step is BM tracking, which estimates BM information (e.q., position and velocity) provided to a missile defense system for the interception purpose.

As in [1], the whole BM flight from launching to impacting on the ground typically experiences three different flight phases: boost, coast and reentry. During those phases, the movement characteristics of the BM are significantly different. Dynamic models corresponding to BM movement

Email addresses: m.yu@lboro.ac.uk (Miao Yu), w.chen@lboro.ac.uk (Wen-Hua Chen), Jonathon.Chambers@newcastle.ac.uk (Jonathon Chambers)

characteristics within different phases have been illustrated in details in [1], based on which various of methods have been developed for the BM tracking in different phases.

Li *et al.* [2] proposed a Maximum Likelihood (ML) algorithm for estimating the launch point of the BM as well as its position and velocity at a particular acquisition time, using the profile-based modeling of the missile boost phase and the line-of-sight (LOS) measurements. A kind of adaptive filter algorithm is proposed in [3] for the boost-phase trajectory estimation. A polynomial model is suggested and the corresponding process noise variance is constructed to make sure that the state estimation error approximates the error lower bound of the optimal estimation. In [4], a trajectory tracking algorithm in the boost phase was proposed based on MLE-CKF federated filter. Unlike the traditional methods (e.g. the Kalman filtering based ones), the estimation of motion state and motion model parameters were separated by using maximum likelihood estimation (MLE) and cubature Kalman filtering (CKF) method. Monte-Carlo simulation results showed the estimation results of the proposed algorithm are superior to the traditional joint estimation based algorithms in both the motion state and motion model parameters. Besides, in order to achieve stably tracking the ballistic target and better adaptability to the flicker noise in the boost phase, a multiple model based method which combines the unscented Kalman filter and unscented particle filter as in [5] is proposed for tracking the ballistic missile in the boost phase.

There are also works related to the ballistic missile tracking in other phases. Tracking of the BM in the coast phase is proposed in [6]. The coast dynamic model is applied and sensor mechanism is modeled to deal with the lag due to the mechanism of data collection and transmission. Both the dynamics and measurement models are incorporated into the extended Kalman filter (EKF) for the BM state estimation. In the approach proposed in [7] for the coast phase tracking, the Doppler frequency is also taken into account for new measurement information. Different from the traditional Kalman filtering based approach, a unscented Kalman filtering (UKF) filtering approach is exploited for tracking. An extended interval Kalman filter approach [8] and sequential Monte Carlo based approach [9] have also been investigated for the reentry phase, where the effect of atmospheric drag is included in the corresponding reentry dynamic model. Furthermore, a comparison study between different filtering methods for BM tracking during the reentry phase is presented in [10]. From the numerical simulation results, it was shown that the Rao-Blackwellised particle filter achieves the best performance, especially when large initial uncertainties exist. In order to compensate for the nonlinear and non-Gaussian problems in the reentry phase tracking, a novel chaos map particle filter (CMPF) [11] is used to estimate the target state. Comparison results show its better performance over the traditional tracking methods such as EKF, UKF and generic particle filter.

In order to accurately track the whole trajectory of the BM, multiple state models need to be considered in the development of tracking algorithms as the BM experiences different flight phases from the launch to impact as mentioned earlier. The most widely-used method for multiple model-based BM tracking is the interacting multiple model (IMM) method (e.q. [12, 13, 14, 15]). Multiple filters corresponding to different state models have been applied in the IMM algorithms, and the state estimation is given by three steps: interaction, filtering and combination as in [16]. However, the traditional IMM method uses *constant* transition probabilities between different models. This is not realistic modeling of BM behavior as the transitions between different phases are related with the states, that is, state dependent. For example, the higher the BM, the more likely the BM flight phase transits from boost to coast. Besides, the EKF-based implementation of the IMM used in the aforementioned works [12, 13, 14, 15] has a limitation in dealing with highly nonlinear BM movement models and measurement models.

For the aforementioned method, it is always assumed that 'perfect' measurements are obtained. That is, the BM could always be correctly detected by a radar sensor without miss detections/false alarms. A more realistic low-observable scenario is considered in [17]and [18], in which 'imperfect' measurements are obtained with both miss detections and false alarms occurring due to the low signal-to-noise ratio (SNR) of a radar sensor. The probabilistic data association (PDA) algorithm is applied in conjunction with other techniques, such as the maximum likelihood (ML) for the data association and ballistic missile state estimation in such a cluttered environment.

In this work, a new method is proposed for tracking the whole trajectory of a BM in a low-observable environment with both miss detections and false alarms, while exploiting domain knowledge in a comprehensive way. First, we consider that a BM could experience different phases and multiple models are thus applied to deal with different movement characteristics. However, different from traditional multiple model works as in [12, 13, 14, 15], a multiple model framework with state dependent model transition probabilities as in [19] is adopted. In this way, a more accurate modeling of phase transition is achieved by exploiting related domain knowledge. Besides, a random finite set (RFS) theory [20], which has recently been investigated for the ballistic missile tracking [21], is applied to construct a more realistic radar measurement model considering both miss detections and false alarms. Based on the proposed model framework and radar measurement model with miss detection/false alarms, exact Bayesian inferences are performed for the state estimation and a new generalized interacting multiple model particle filtering (denoted as G-IMMPF) is developed for the implementation of related inferences. The G-IMMPF algorithm is an extension of the traditional interacting multiple model particle filtering (IMMPF) in [19], by incorporating a more realistic random finite set (RFS) based measurement likelihood function to deal with both

miss detections and false alarms.

The structure of this paper is as follows: Section 2 describes the models used in the BM tracking. An illustration of the proposed method is presented in Section 3, which explains both the Bayesian inference and the developed G-SD-IMMPF algorithm for the related implementation. Comprehensive numerical simulation studies with different algorithms are presented in Section 4, and the final conclusions are given in Section 5.

2. Ballistic missile tracking models

2.1. A multiple modeling framework with state dependent transition probabilities

As illustrated in Fig. 1, the entire trajectory of the BM from launch to impact is commonly divided into three phases [1, 22]:

Boost phase: a BM experiences a powered, endo-atmospheric flight which lasts from launch to thrust cutoff;

Coast phase: the thruster of a BM is turned off and the missile flies freely subject to little atmospheric drag because it is in a relatively high part of the atmosphere;

Reentry phase: a BM reaches the lower part of the atmosphere and the atmospheric drag becomes considerable again and lasts until its impact to the ground.

In order to model missile movements in different phases, three different models including boost model, coast model and reentry model are applied for the BM tracking (details of the BM models used in this paper are shown in the Appendix).

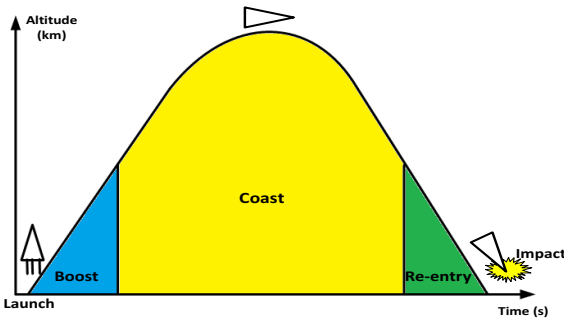

Figure 1: The illustration of the entire trajectory and different phases of the BM.

Traditionally, a multiple modeling system proposed in [12, 13, 14, 21] is applied. As illustrated in Fig. 2(a), in such a system, the flight mode (boost, coast and reentry) at a particular time only depends on its predecessor at the previous time instance. Transition probabilities between different modes are set to be constant. However, in reality the actual BM flight mode may be also dependent on some state (position/velocity) information. For example, as the height of the BM increases,it is

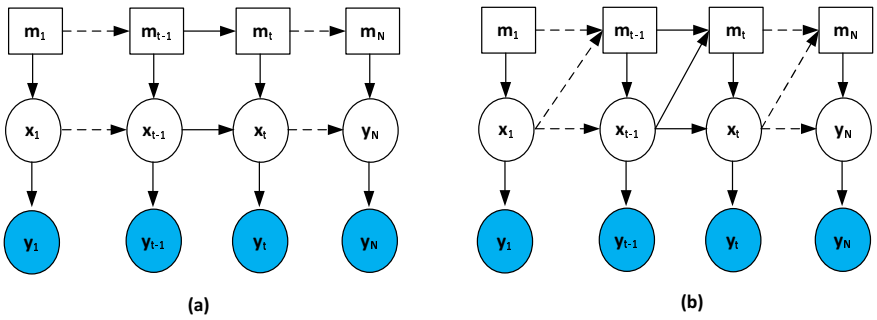

Figure 2: The structure of a multiple modeling framework with constant mode transition probabilities (a) and that with state dependent mode transitions (b), with m_t, $\mathbf{x}_t$ and $\mathbf{y}_t$ representing the movement mode, state and measurement, respectively.

more likely for a BM to transit from the boost to coast phase. To reflect this, a modeling system as illustrated in Fig. 2(b) is applied with the particular movement mode at a time instance being also dependent on the previous state. Thus state dependent transition probabilities rather than constant ones shall be used to better represent the physical characteristic of a BM.

Different types of domain knowledge are now exploited to determine the state-dependent mode transition probabilities in this work. One type of domain knowledge is about the mode transition related to the BM altitude. As mentioned in [1], the transition between the boost to coast phase is related to the altitude of the BM. When the height reaches a particular threshold, the thruster of a BM is turned off and the flight phase transits to the coast phase, as illustrated in Fig. 3(a). Another type of domain knowledge is that as the missile flies in the coast phase, it first reaches a peak and then drops towards the ground (due to the effect of the gravity) while the altitude decreases and the angle between the velocity vector and gravity force also decreases due to the effect of gravity. When both the height and angle between the velocity vector and gravity force drop to certain values, the BM reenters the low part of the atmosphere and transits to the reentry phase, as illustrated in Fig. 3(b).

The aforementioned domain knowledge, which reflects phase transitions, is represented as follows:

$$\begin{aligned} &m_t = coast, \quad if \quad h_{t-1} > h_1 \quad \text{and} \quad m_{t-1} = boost \\ &m_t = reentry, \quad if \quad h_{t-1} < h_2 \quad \text{and} \quad \theta_{t-1} < \theta_1 \quad \text{and} \quad m_{t-1} = coast, \end{aligned} \tag{1}$$

where m_t denotes the state model index (*boost*, *coast* or *reentry*). The parameters h_t and θ_t represent respectively the ballistic missile height and the angle between the missile velocity and gravity force; h_1, h_2 and θ_1 represent threshold values. Normally, the exact values of h_1, h_2 and θ_1 are unknown, but some information could be obtained from previously collected information (e.g.

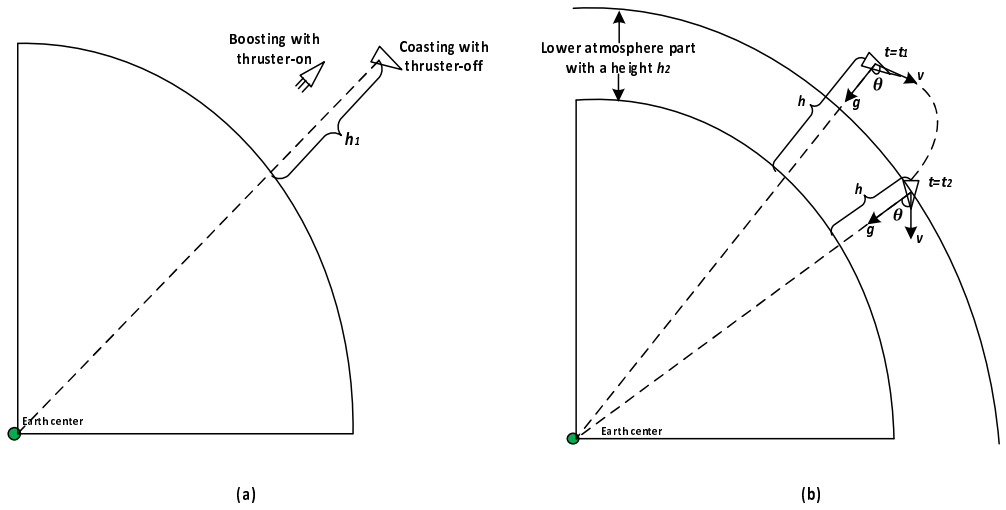

Figure 3: The the BM flight modes transitions between different phases: (a). The BM transits from boost to coast when it reaches a certain threshold with thruster being off (b). As the BM approaches the lower part of the atmosphere from time t_1 to t_2, the height h and angle θ (between the velocity vector v and gravity force vector g) reduce.

the database for a particular missile type). The more information we obtain, the more accurate values can be obtained with less uncertainties.

To consider the uncertainties of h_1, h_2 and θ_1, the Gaussian distribution could be exploited to model them in a convenient way as:

$$\begin{aligned} h_1 &\sim N(\cdot|m_{h_1}, \sigma^2_{h_1}) \\ h_2 &\sim N(\cdot|m_{h_2}, \sigma^2_{h_2}) \\ \theta_1 &\sim N(\cdot|m_{\theta_1}, \sigma^2_{\theta_1}) \end{aligned} \tag{2}$$

where m_{h_1}, m_{h_2} and m_{θ_1} represent the guess of the true values of h_1, h_2 and θ_1, whilst σ_{h_1}, σ_{h_2} and σ_{θ_1} are the standard deviations, which represent the uncertainties for the height and angle thresholds.

Combining (1) and (2), the transition probabilities from the boost to coast and from the coast to reentry are modeled as (3)

$$\begin{aligned} p(m_t = coast|m_{t-1} = boost, h_{t-1}) &= p(h_{t-1} > h_1) = CDF(h_{t-1}|m_{h1}, \sigma^2_{h1}) \\ p(m_t = reentry|m_{t-1} = coast, h_{t-1}, \theta_{t-1}) &= p(h_{t-1} < h_2, \theta_{t-1} < \theta_1) \\ &= (1 - CDF(h_{t-1}|m_{h2}, \sigma^2_{h2})) \cdot (1 - CDF(\theta_{t-1}|m_{\theta_1}, \sigma^2_{\theta_1})), \end{aligned} \tag{3}$$

where $CDF(\cdot|m, std^2)$ is the cumulative density function for a Gaussian distribution with the mean m and standard deviation σ.

In this way, instead of traditional constant transition probabilities, flight mode transitions are modeled in a state dependent way (related to the height and angle information as in (3)) by incorporating proper domain knowledge to reflect the realistic BM flight characteristics.

2.2. Measurement model in a low-observable environment

Traditional measurement models in most of current BM tracking works have an unrealistic assumption that the BM can always be perfectly measured. However, both miss detections and false alarms exist in a low-observable environment, due to the low signal-to-noise ratio (SNR) as in [23]. In this work, a more realistic measurement model is applied to deal with such miss detections and false alarms by representing the measurement set (denoted as $\mathbf{Z}$) as a union of two independent random finite sets (RFS) [24], which is given by

$$\mathbf{Z} = \mathbf{C} \bigcup \mathbf{W}, \tag{4}$$

where $\mathbf{W}$ represents the RFS due to the object of interest while $\mathbf{C}$ denotes the RFS of false detections.

With a probability of P_d between 0 and 1, it is assumed that a radar measures the range r_t^m, azimuth angle θ_t^m and elevation angle φ_t^m of a BM in a local east-north-up (ENU) coordinate system [22]. Thus the RFS $\mathbf{W}$ could either be empty or a singleton vector $\{r_t^m, \theta_t^m, \varphi_t^m\}$ representing the object measurements.

2.2.1. Object measurements

The ENU coordinate system has the origin at the radar position, with three axes being towards the east, north and up directions, respectively. The global earth-centered-earth-fixed (ECEF) [22] and local ENU coordinate systems are illustrated in Fig. 4, and the corresponding coordinates can be converted through:

$$\begin{bmatrix} p_t^{x,l} \\ p_t^{y,l} \\ p_t^{z,l} \end{bmatrix} = M \cdot \left(\begin{bmatrix} p_t^{x} \\ p_t^{y} \\ p_t^{z} \end{bmatrix} - \mathbf{p}^R \right) \tag{5}$$

where $\left[p_t^{x,l}, p_t^{y,l}, p_t^{z,l}\right]^T$ represents the local ENU coordinate of the radar, $\mathbf{p}^R = \left[p^{x,R}, p^{y,R}, p^{z,R}\right]^T$ the position of the radar in the ECEF coordinate system, and M the rotation matrix defined by:

$$M = \begin{bmatrix} -sin(\lambda) & cos(\lambda) & 0 \\ -cos(\lambda)sin(\phi) & -sin(\lambda)sin(\phi) & cos(\phi) \\ cos(\lambda)cos(\phi) & sin(\lambda)cos(\phi) & sin(\phi) \end{bmatrix} \tag{6}$$

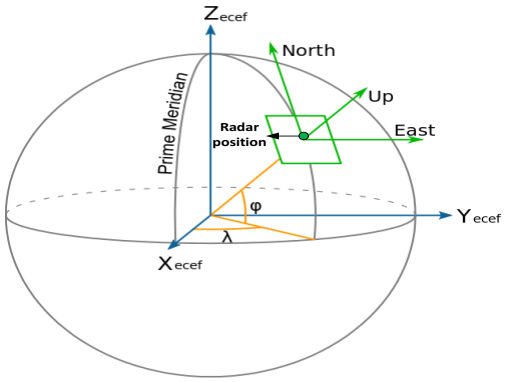

Figure 4: The illustration of the global ECEF and local ENU coordinate systems. Note, the x and y axes of the ECEF coordinate system lie in the equatorial plane while the x axis pointing towards the Greenwich. And the z-axis of the ECEF coordinate system is the conventional terrestrial pole (CTP) axis

with ϕ and λ being the latitude and longitude of the radar.

Under the local ENU coordinate system, the measurement equation for the range, azimuth angle and elevation angle is described as:

$$\begin{bmatrix} r_t^m \\ \theta_t^m \\ \varphi_t^m \end{bmatrix} = h(\mathbf{x}_t^s) + \mathbf{n}_t^m = \begin{bmatrix} \sqrt{(p_t^{x,l})^2 + (p_t^{y,l})^2 + (p_t^{z,l})^2} \\ \arctan(\frac{p_t^{x,l}}{p_t^{y,l}}) \\ \arctan(\frac{p_t^{z,l}}{\sqrt{(p_t^{x,l})^2 + (p_t^{y,l})^2}}) \end{bmatrix} + \mathbf{n}_t^m \tag{7}$$

where $\mathbf{x}_t^s$ represents the state vector for a particular mode s, which can be boost, coast or reentry, and $\mathbf{n}_t^m$ a measurement noise vector.

2.2.2. False detections

As in [24], typically the number of false detections in the RFS set $\mathbf{C}$ is modeled by the Poisson distribution as:

$$P(|C| = s) = \frac{e^{-\lambda}\lambda^s}{s!} \tag{8}$$

where λ is the excepted value of false alarm number. Furthermore, conditioned on the number $|C|$, false detections are modeled as independent, identically distributed (IID) random vectors taking values from the feasible measurement space.

Following these two assumptions, the probability density function (PDF) of the RFS $\mathbf{C}$ can be given by (detailed derivations are referred in [24])

$$\kappa(\mathbf{C}) = e^{-\lambda}\Pi_{\mathbf{z}\in\mathbf{C}}\lambda u(\mathbf{z}) \tag{9}$$

where $\mathbf{z}$ is a measurement in the RFS $\mathbf{C}$ and $u(\cdot)$ represents the uniform distribution defined in the feasible measurement space.

3. Generalized state dependent interactive multiple model particle filtering

Based on both the BM modeling and RFS measurement model as defined in the previous section, a generalized state dependent interacting multiple model particle filtering (G-SD-IMMPF) algorithm is developed for ballistic missile tracking. Compared with the conventional multiple model filtering method for the BM tracking in [12, 13, 14], the proposed algorithm adopts the multiple model framework with state dependent transition probabilities. Moreover, particle filtering is applied to cope with the non-linearity of both state and measurement models for the BM tracking problem. Compared with the original SD-IMMPF method in [19], the developed algorithm also incorporates a generalized measurement likelihood function based on the RFS theory into the Bayesian inference framework, in order to cope with both miss detections and false alarms in a more effective way.

The proposed G-SD-IMMPF algorithm is based on the exact Bayesian inference framework for a multiple model system, and its overall process is divided into four steps:

$$p(m_{t-1}|\mathbf{Z}_{t-1}) \xrightarrow{\text{Mixing}} p(m_t|\mathbf{Z}_{t-1}) \tag{10}$$

$$p(\mathbf{x}_{t-1}|m_{t-1}, \mathbf{Z}_{t-1}) \xrightarrow{\text{interact}} p(\mathbf{x}_{t-1}|m_t, \mathbf{Z}_{t-1}) \tag{11}$$

$$p(\mathbf{x}_{t-1}|m_t, \mathbf{Z}_{t-1}) \xrightarrow{\text{Evolutions}} p(\mathbf{x}_t|m_t, \mathbf{Z}_{t-1}) \tag{12}$$

$$p(\mathbf{x}_t|m_t, \mathbf{Z}_{t-1}) \xrightarrow{\text{Correction}} p(\mathbf{x}_t, m_t|\mathbf{Z}_t) \tag{13}$$

where m_t represents the model index (*boost*, *coast* or *reentry*), $\mathbf{x}_t$ the state vector and $\mathbf{Z}_t$ the obtained measurements at time instance t, which may include both miss detections and false alarms.

3.1. Detailed Bayesian inference procedure

The detailed Bayesian inferences for the four steps are described as follows.

3.1.1. Mode mixing:

The mode mixing is related to the evolution of the model probability between consecutive discrete time instances $t-1$ and t. Using the law of total probability, we have:

$$p(m_t = s|\mathbf{Z}_{t-1}) = \sum_{r\in\mathcal{M}} p(m_t = s, m_{t-1} = r|\mathbf{Z}_{t-1}) = \sum_{r\in\mathcal{M}} p(m_t = s|m_{t-1} = r, \mathbf{Z}_{t-1})p(m_{t-1} = r|\mathbf{Z}_{t-1}),$$
$$\forall s, r \in \mathcal{M} = \{boost, coast, reentry\}, \tag{14}$$

where $p(m_t = s|m_{t-1} = r, \mathbf{Z}_{t-1})$ which can further be decomposed as:

$$p(m_t = s|m_{t-1} = r, \mathbf{Z}_{t-1}) = \int \pi_{rs}(\mathbf{x}_{t-1}) \cdot p(\mathbf{x}_{t-1}|m_{t-1} = r, \mathbf{Z}_{t-1})\, \mathrm{d}\mathbf{x}_{t-1} \tag{15}$$

and $\pi_{rs}(\mathbf{x}_{t-1})$ represents the state-dependent model transition probability between models r and s as discussed in the last section.

3.1.2. State interacting:

State interaction generates the initial mode-conditioned density $p(\mathbf{x}_{t-1}|m_t = s, \mathbf{Z}_{t-1})$ according to the conditional probability relation and the law of total probability as:

$$p(\mathbf{x}_{t-1}|m_t = s, \mathbf{Z}_{t-1}) = \frac{\sum_{r\in\mathcal{M}} \pi_{rs}(\mathbf{x}_{t-1}) \cdot p(\mathbf{x}_{t-1}, m_{t-1} = r|\mathbf{Z}_{t-1})}{p(m_t = s|\mathbf{Z}_{t-1})}. \tag{16}$$

3.1.3. Evolution:

The state evolution step is to propagate the mode-conditioned state density from $t-1$ to t. Given the initial density is provided in Eq. (16), the mode-conditioned prior distribution $p(\mathbf{x}_t|m_t = s, \mathbf{Z}_{t-1})$ at t is calculated as:

$$p(\mathbf{x}_t|m_t = s, \mathbf{Z}_{t-1}) = \int p(\mathbf{x}_t|\mathbf{x}_{t-1}, m_t = s, \mathbf{Z}_{t-1})p(\mathbf{x}_{t-1}|m_t = s, \mathbf{Z}_{t-1})\mathrm{d}\mathbf{x}_{t-1} \tag{17}$$

where $p(\mathbf{x}_t|\mathbf{x}_{t-1}, m_t = s, \mathbf{Z}_{t-1})$ is the transition probability depending on a particular state model $m_t = s$ (details of state models are provided in the Appendix).

3.1.4. Correction:

Generalized likelihood function: According to Eq. (4), a measurement set $\mathbf{Z}$ is represented as a union of two independent RFS. Based on the convolution formula for the RFS statistics calculus as in [24] and the possible value of RFS $\mathbf{W}$ representing the object of interest measurement, the

corresponding conditional probability density function (PDF) for the measurement set at time instant t can be estimated as:

$$p(\mathbf{Z}_t|\mathbf{x}_t) = \sum_{\mathbf{z}_t \subseteq \mathbf{Z}_t} \eta(\mathbf{z}_t|\mathbf{x}_t)\kappa(\mathbf{Z}_t \backslash \mathbf{z}_t), \tag{18}$$

where $\mathbf{z}_t$ could either be empty or a single measurement in the measurement set $\mathbf{Z}_t$, '\' denotes the set-difference operation, and $\eta(\mathbf{z}_t|\mathbf{x}_t)$ is defined according to [24] as:

$$\eta(\mathbf{z}_t|\mathbf{x}_t) = \begin{cases} 1 - P_d & \mathbf{z}_t = \emptyset \\ P_d g(\mathbf{z}_t|\mathbf{x}_t) & otherwise \end{cases} \tag{19}$$

where $g(\mathbf{z}_t|\mathbf{x}_t)$ is the (conventional) measurement likelihood function of measurement $\mathbf{z}_t$ due to the object in state $\mathbf{x}_t$. For the BM tracking in this work, it is a Gaussian distribution determined by (7).

By combining (9), (18) and (19), we can obtain the following generalized likelihood function:

$$\begin{aligned} p(\mathbf{Z}_t|\mathbf{x}_t) &= \eta(\emptyset|\mathbf{x}_t) \cdot \kappa(\mathbf{Z}_t) + \sum_{\mathbf{z}_t \subseteq \mathbf{Z}_t} \eta(\mathbf{z}_t|\mathbf{x}_t) \cdot \kappa(\mathbf{Z}_t \backslash \mathbf{z}_t) \\ &= \kappa(\mathbf{Z}_t)[1 - P_d + P_d \sum_{\mathbf{z}_t \subseteq \mathbf{Z}_t} \frac{g(\mathbf{z}_t|\mathbf{x}_t)\kappa(\mathbf{Z}_t \backslash \mathbf{z}_t)}{\kappa(\mathbf{Z}_t)}] \\ &= \kappa(\mathbf{Z}_t)[1 - P_d + P_d \sum_{\mathbf{z}_t \subseteq \mathbf{Z}_t} \frac{g(\mathbf{z}_t|\mathbf{x}_t)}{\lambda c(\mathbf{z}_t)}]. \end{aligned} \tag{20}$$

Bayesian updating:

The obtained generalized likelihood function is then applied to correct the prior by Bayes rule as:

$$p(\mathbf{x}_t, m_t = s|\mathbf{Z}_t) \propto p(m_t = s|\mathbf{Z}_{t-1})p(\mathbf{x}_t|m_t = s, \mathbf{Z}_{t-1})p(\mathbf{Z}_t|\mathbf{x}_t), \tag{21}$$

which is posterior distribution based on the current measurement set and summarizes both the state and mode information at the current time instance.

3.2. G-SD-IMMPF implementation

Since there is no analytical solution for the above Bayesian inference framework due to the nonlinearity and non-Gaussian distribution of both the state and measurement models, a particle filtering-based approach is proposed to implement the aforementioned Bayesian inference of the modeling system with a generalized measurement likelihood function to deal with both miss

detection and false alarms.

Initially, it starts at time $t-1$ with the set of weighted particles $\{\mathbf{x}_{t-1}^{r,k}, w_{t-1}^{r,k}; r \in \mathcal{M}, k \in \{1,\ldots,N\}\}$ to approximate the probability $p(\mathbf{x}_{t-1}, m_{t-1} = r|\mathbf{Z}_{t-1})$. Based on this, the Bayesian inference procedure is implemented by the G-SD-IMMPF algorithm as follows.

Mode mixing implementation: By using a set of particles, prior mode probability in (14) can be approximated as:

$$p(m_t = s|\mathbf{Z}_{t-1}) \approx \sum_{r\in\mathcal{M}} \sum_{k=1}^{N} \pi_{rs}(\mathbf{x}_{k-1}^{r,k}) \cdot w_{t-1}^{r,k} \triangleq \Lambda_{t-1}^{s}, \tag{22}$$

where Λ_{t-1}^{s} is defined to facilitate the rest of the derivation.

State interacting implementation: The state interaction process can be implemented by inserting particles at $t-1$ with the different mode index r into Eq. (16) such that

$$p(\mathbf{x}_{t-1}|m_t = s, \mathbf{Z}_{t-1}) \approx \sum_{r\in\mathcal{M}} \sum_{k=1}^{N} \pi_{rs}(\mathbf{x}_{t-1}^{r,k}) w_{t-1}^{r,k} \delta(\mathbf{x}_{t-1} - \mathbf{x}_{t-1}^{r,k}) / \Lambda_{t-1}^{s}. \tag{23}$$

In order to cumbersome the problem of increasing number of particles from N to $N \times |\mathcal{M}|$ (where $|\mathcal{M}|$ represents the number of modes) which will also lead to the exponentially increasing of particles in the following time instances, a resampling procedure as in [19] is performed. A set of N particles $\{\mathbf{x}_{t-1}^{s,k}\}_{k=1,\ldots,N}$ is sampled according to the distribution representation in (23) for approximating $p(\mathbf{x}_{t-1}|m_t = s, \mathbf{Z}_{t-1})$. In this way, the number of particles for approximating the related distribution will not increase.

Evolution implementation: The third step is the particles' evolution from time $t-1$ to t. Resampled particle set $\{\mathbf{x}_{t-1}^{s,k}\}_{k=1,\ldots,N}$ could be evolved to generate a new particle set $\{\mathbf{x}_{t}^{s,k},\}_{k=1,\ldots,N}$ to approximate the distribution $p(\mathbf{x}_t|m_t = s, \mathbf{Z}_{t-1})$ according to (24). As mentioned in [19], for every $\mathbf{x}_t^{s,k}$, it is obtained from sampling the related transition distribution $p(\mathbf{x}_t|m_t = s, \mathbf{x}_{t-1}^{s,k}, \mathbf{Z}_{t-1})$.

$$p(\mathbf{x}_t|m_t = s, \mathbf{Z}_{t-1}) \approx \frac{1}{N} \sum_{k=1}^{N} \delta(\mathbf{x}_t - \mathbf{x}_t^{s,k}). \tag{24}$$

Correction implementation: By inserting (22) and (24) into (21), we have:

$$p(\mathbf{x}_t, m_t|\mathbf{Z}_t) \propto \sum_{k=1}^{N} \frac{\Lambda_{t-1}^{s}}{N} p(\mathbf{Z}_t|\mathbf{x}_t^{s,k}) \delta(\mathbf{x}_t - \mathbf{x}_t^{s,k}) \tag{25}$$

According to the definition of the generalized likelihood function as in (20) , we have:

$$p(\mathbf{x}_t, m_t = s|\mathbf{Z}_t) \propto \sum_{k=1}^{N} w_t^{s,k} \delta(\mathbf{x}_t - \mathbf{x}_t^{s,k}), \quad with \quad w_t^{s,k} = \Lambda_{t-1}^{s} \kappa(\mathbf{Z}_t)[1 - P_d + P_d \sum_{\mathbf{z}_t \subseteq \mathbf{Z}_t} \frac{g(\mathbf{z}_t|\mathbf{x}_t^{s,k})}{\lambda c(\mathbf{z}_t)}]. \quad (26)$$

The weights are finally normalized to make $\sum_s \sum_{k=1}^{N} w_t^{s,k} = 1$. The posterior distribution $p(\mathbf{x}_t, m_t = s|\mathbf{Z}_t)$ for the mode s is then approximated by a set of weights $\{w_t^{s,k}\}_{k=1,\ldots,N}$ and particles $\{\mathbf{x}_t^{s,k}\}_{k=1,\ldots,N}$ (the same procedure for implementing mode mixing, intersection, evolution and correction is applied for every mode). Finally, both the state estimation (denoted as $\hat{\mathbf{x}}_t$) and mode probability can be estimated from related particles and weights as:

$$\hat{\mathbf{x}}_t = \sum_{s \in \mathcal{M}} \sum_{i=1}^{N} w_t^{i,s} \mathbf{x}_t^{i,s} \quad (27)$$

$$p(m_t = s) = \sum_{i=1}^{N} w_t^{i,s} \quad (28)$$

4. Numerical simulation studies

4.1. Experimental scenario setting

In this section, numerical simulation studies are performed to analyse the performance of the proposed G-SD-IMMPF method for the BM tracking. An entire BM trajectory is simulated in the ECEF coordinate system as in Fig. 5. Key parameters of the simulated BM flight trajectory are listed in Table I, which corresponds to the short range ballistic missile as described in [25]. Based on the simulated BM trajectory, algorithms can be applied for the BM tracking, with the following settings.

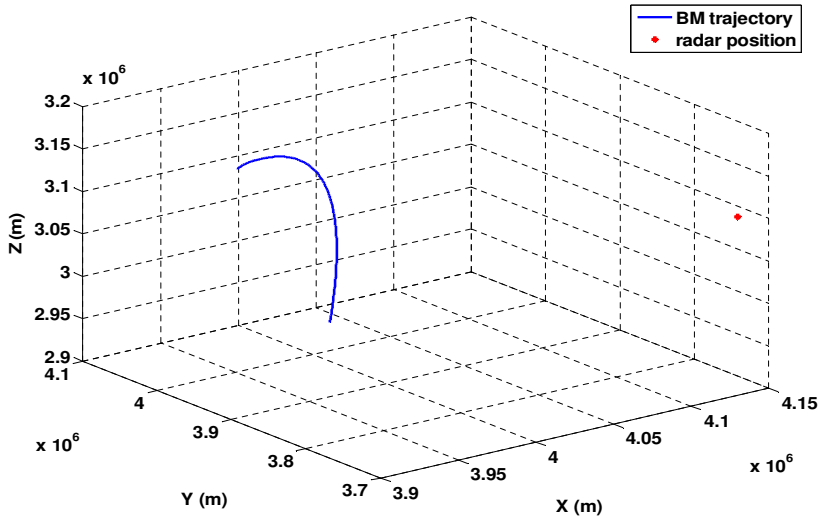

Figure 5: Simulated BM trajectory and radar position in the ECEF coordinate system

Table 1: The parameters of the simulated BM trajectory

Flight time	Range	Boost time	Engine-off velocity
305 (s)	292 (km)	66 (s)	1.46 (km/s)

Initialisation: Considering the uncertainty about both the initial position and velocity of a tracked BM, Gaussian distributions are applied to model the initial position $\mathbf{p}_0$ and velocity $\mathbf{v}_0$ of the BM in the ECEF coordinate system as:

$$\mathbf{p}_0 \sim N(\cdot|\overline{\mathbf{p}}_0, \Sigma_0^{\mathbf{p}}), \quad \mathbf{v}_0 \sim N(\cdot|\overline{\mathbf{v}}_0, \Sigma_0^{\mathbf{v}}) \tag{29}$$

where the means $\overline{\mathbf{p}}_0$ and $\overline{\mathbf{v}}_0$ represent the initial guess of the true position and velocity, respectively and Σ_0^p and Σ_0^v the associated uncertainties, in this work they are defined as:

$$\Sigma_0^{\mathbf{p}} = \begin{bmatrix} 100, & 0, & 0 \\ 0, & 100, & 0 \\ 0, & 0, & 100 \end{bmatrix} (m), \quad \Sigma_0^{\mathbf{v}} = \begin{bmatrix} 1, & 0, & 0 \\ 0, & 1, & 0 \\ 0, & 0, & 1 \end{bmatrix} (m/s) \tag{30}$$

We model $\overline{\mathbf{p}}_0$ and $\overline{\mathbf{v}}_0$ as:

$$\overline{\mathbf{p}}_0 = \mathbf{p}_0^s + \mathbf{w}_p, \quad \overline{\mathbf{v}}_0 = \mathbf{v}_0^s + \mathbf{w}_v \tag{31}$$

where $\mathbf{p}_0^s$ and $\mathbf{v}_0^s$ are the position and velocity of the simulated trajectory at $t = 0$, and $\mathbf{w_p}$ and $\mathbf{w_v}$ introduced noisy terms controlling the accuracies of the initial observation/guess. In this work, $\mathbf{w_p}$ and $\mathbf{w_v}$ are set to follow Gaussian distributions with non-zero means of $\bar{\mathbf{w}}_\mathbf{p} = \begin{bmatrix} 10 \\ 10 \\ 10 \end{bmatrix}$ and $\bar{\mathbf{w}}_\mathbf{v} = \begin{bmatrix} 1 \\ 1 \\ 1 \end{bmatrix}$, as well as covariances of $\Sigma_0^{\mathbf{p}}$ and $\Sigma_0^{\mathbf{v}}$ as defined previously.

State and measurement models: Three state models corresponding to boost, coast and reentry phases are applied for the BM tracking and the details of these models are provided in Appendix. As mentioned in Section 2, the proposed modeling system is applied with state dependent transition probabilities between boost to coast as well as coast to reentry. Based on these transition probabilities and some other movement characteristics of a BM (i,e., a BM can not transit from the coast phase to the boost phase) , a full mode transition matrix is shown as

$$
\begin{array}{c} \\ boost \\ coast \\ reentry \end{array}
\begin{array}{c}
\begin{array}{ccc} boost & coast & reentry \end{array} \\
\begin{pmatrix}
1-p_1(h_t) & p_1(h_t) & 0 \\
0 & 1-(1-p_2(h_t))\cdot(1-p_1(\theta_t)) & (1-p_2(h_t))\cdot(1-p_1(\theta_t)) \\
0 & 0 & 1
\end{pmatrix}
\end{array}, \tag{32}
$$

where $p_1(h_t) = CDF(h_t|m_{h1}, std_{h1})$, $p_2(h_t) = CDF(h_t|m_{h2}, std_{h2})$ and $p_1(\theta_t) = CDF(\theta_t|m_{\theta_1}, std_{\theta_1})$. Related parameters are set as: $m_{h1} = 35000$ (m), $m_{h2} = 25000$ (m), $\sigma_{h1} = \sigma_{h2} = 3000$ (m), $m_{\theta_1} = 0.85$ (rad) and $\sigma_{\theta_1} = 0.2$ (rad) in this work.

It is assumed that the radar measures the BM with a detection probability of 90%. The related object measurement is modeled according to (7), with the measurement noises being:

$$
\mathbf{n}_t^m \sim N(\cdot|\mathbf{0}_{3\times1}, \Sigma_m), \tag{33}
$$

where

$$
\Sigma_m = diag([(100)^2\ (m)^2, (0.1)^2\ (rad)^2, (0.1)^2\ (rad)^2]). \tag{34}
$$

The number of false alarms satisfies a Poisson distribution with the expected number of false alarms λ in (8) being 10. Conditioned on the expected number, the false alarm measurements are distributed uniformly among the measurement space.

4.2. Algorithm evaluation

Based on the aforementioned experimental setting, the proposed G-SD-IMMPF algorithm is tested and compared with other algorithms, with 1×10^4 particles being applied for every state model. Firstly, the algorithm is compared with the traditional SD-IMMPF algorithm in [19], to show its advantage to incorporate the RFS based generalized measurement likelihood function. Note, different from the proposed method, the traditional SD-IMMPF algorithm only exploits one measurement for the correction procedure. In order to find the most suitable measurement to be applied in the SD-IMMPF algorithm, the nearest neighbor data association method as in [26] is applied.

100 Monte Carlo simulations are made and the comparison results are shown in Fig. 6 and Tables 2 and 3, from which we can see that the proposed method achieves much better performance than the traditional SD-IMMPF one, during different BM flight phases including both time periods after flight mode transition occurs and the one when the BM flights 'stable' following the coast

mode. For the proposed method, the miss detection, object measurement and false alarms are comprehensively considered and modeled in a theoretical way by the RFS theory. However, in the traditional SD-IMMPF method, only one measurement is chosen for updating in an empirical way instead of a comprehensively theoretical modeling. When the object is not detected, some false alarm may be chosen as the 'correct' measurement by the nearest neighbor data association method for updating, which will lead to poor estimation results.

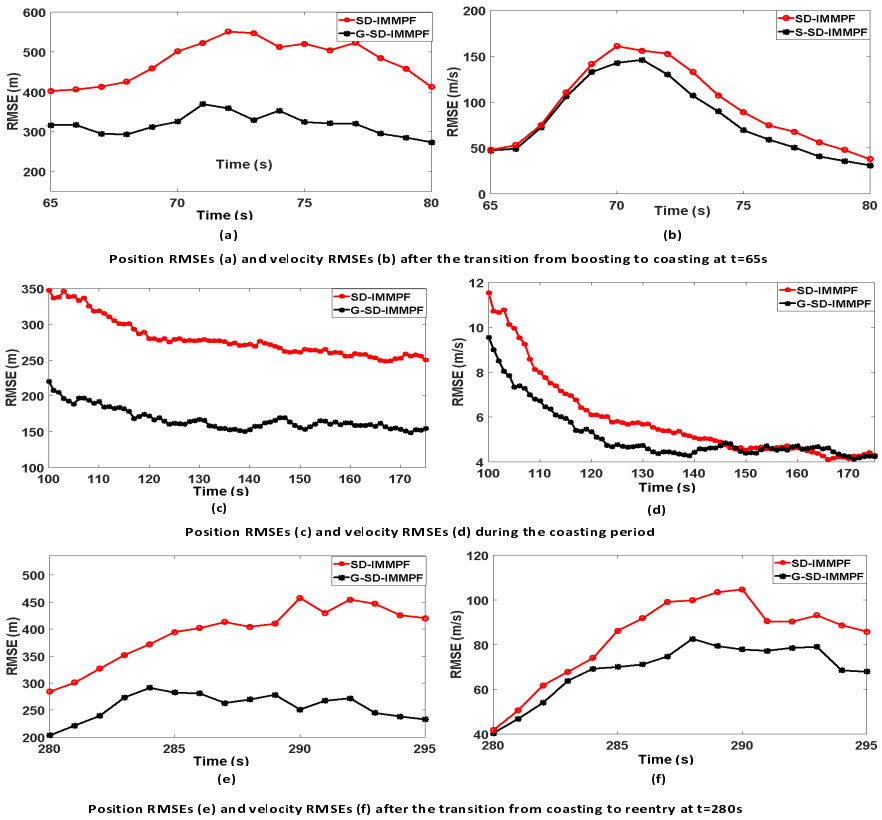

Figure 6: The averaged position and velocity RMSEs curves during different intervals, from 100 Monte carlo simulations by different algorithms

Table 2: The averaged position RMSEs (m) of different phases for 100 Monte Carlo simulations by different algorithms.

	SD-IMMPF	G-SD-IMMPF
Averaged RMSE for 65-80 (s)	443.68	299.14
Averaged RMSE for 100-175 (s)	265.88	170.36
Averaged RMSE for 280-295 (s)	375.90	254.06

Next, we show the comparisons of methods applying different multiple modeling framework, including the constant transition probabilities model (denoted as CTP Model for short) based method as in [12, 13, 14, 15] and the proposed method exploiting state dependent transition probabilities model (denoted as SDTP Model for short). For a fair comparison, the particle filtering method with the same particle sizes and generalized measurement likelihood function is applied.

Table 3: The averaged velocity RMSEs (m/s) of different phases for 100 Monte Carlo simulations by different algorithms.

	SD-IMMPF	G-SD-IMMPF
Averaged RMSE for 65-80 (m/s)	101.72	77.30
Averaged RMSE for 100-175 (m/s)	8.46	6.06
Averaged RMSE for 280-285 (m/s)	81.07	62.98

Fig. 7 shows the estimated mode probabilities by exploiting different models, from which we can see that the mode estimation results are more consistent with the groundtruth ones by the SDTP Model approach thanks to the domain knowledge aided transition probabilities. The better mode estimation results also lead to more accurate estimation of the position and velocity information, as shown in Fig. 8 and Table 4 and 5.

Besides, the computational time of the proposed algorithm is evaluated. 100 Monte-Carlo simulations on an ordinary PC (Intel(R) Core (TM) i5-3570 CPU@3.40 GHz) are performed. On average, it is shown that the time taken for exploiting measurements obtained at a time instance for implementing the G-SD-IMMPF filtering algorithm (as in Section 3.2) is approximately 0.05s.

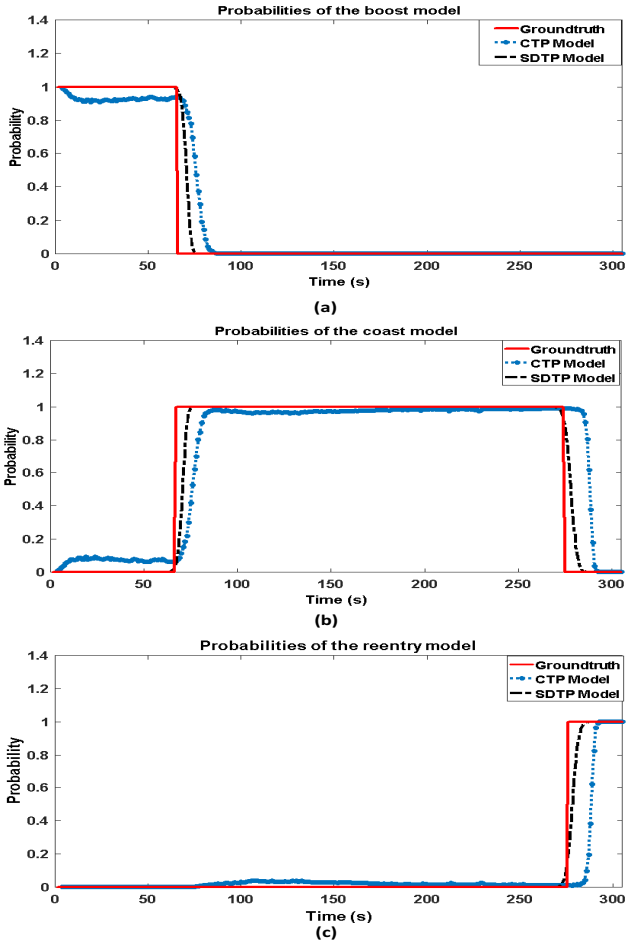

Figure 7: Estimated mode probabilities by CTP and SDTP Models respectively.

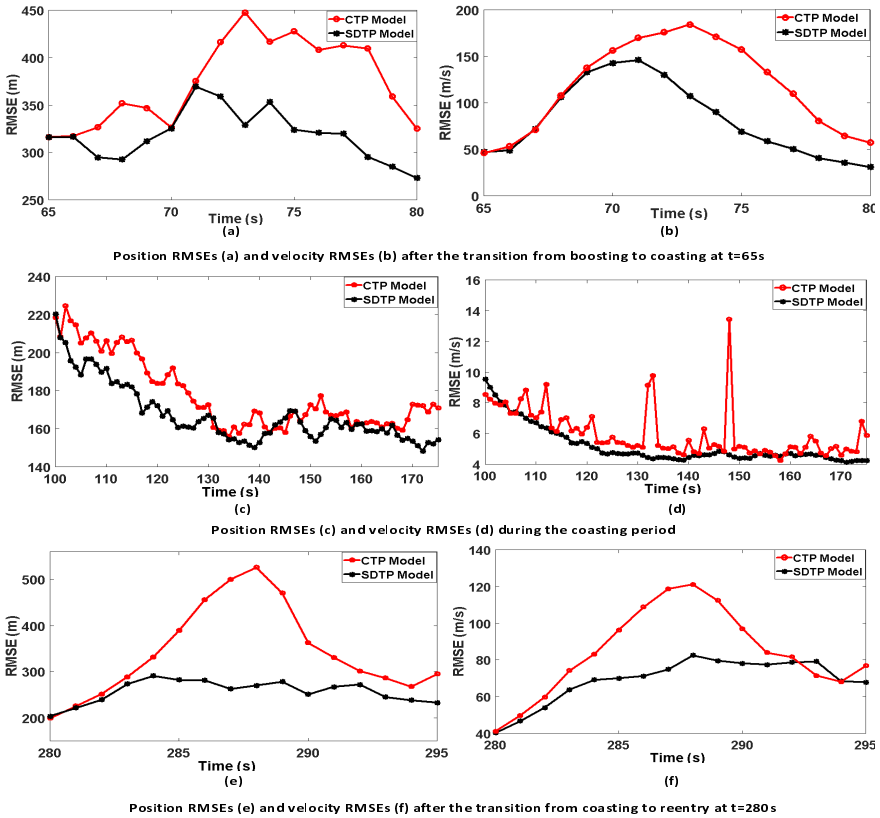

Figure 8: The averaged position and velocity RMSEs curves during different intervals, from 100 Monte carlo simulations by different modeling approaches

Table 4: The averaged position RMSEs (m) of different phases for 100 Monte Carlo simulations by different models.

	CTP Model	SDTP Model
Averaged RMSE for 65-80 (s)	360.35	299.14
Averaged RMSE for 100-175 (s)	175.87	170.36
Averaged RMSE for 280-295 (s)	341.93	254.06

5. Conclusions

In this paper, we have proposed a new G-SD-IMMPF method for tracking the entire trajectory of a ballistic missile while considering both miss detections and false alarms in a low-observable environment. A hybrid system with state dependent transition probabilities is proposed for modeling the realistic BM movement. The measurement set including both miss detection and false alarm is modeled by a RFS, with a generalized measurement likelihood function being calculated by the related RFS theory. By the aid of the generalized measurement likelihood function, the particle

Table 5: The averaged velocity RMSEs (m/s) of different phases for 100 Monte Carlo simulations by different models.

	CTP Model	SDTP Model
Averaged RMSE for 65-80 (m/s)	116.06	77.30
Averaged RMSE for 100-175 (m/s)	7.25	6.06
Averaged RMSE for 280-285 (m/s)	89.83	62.98

filtering based G-SD-IMMPF method is then developed to implement the Bayesian inference for the BM tracking, based on the enhanced hybrid modeling system with state dependent transition probabilities. The simulations showed the advantage of the proposed algorithm for the estimations of both the model probability and state vector components of a BM.

In the future, we will exploit more domain knowledge to model the BM transition probabilities in a more realistic way. Besides, from the algorithm aspect we will exploit variable number of particles for each mode instead of a fixed number (for example, when the probability is low, comparatively small number of particles will be assigned) to increase the algorithm efficiency.

Acknowledgement

This work was supported by the UK Engineering and Physical Sciences Research Council (EPSRC) Grant number EP/K014307/1 and the MOD University Defence Research Collaboration in Signal Processing.

References

[1] X. Li, V. Jilkov, Survey of Maneuvering Target Tracking. Part ii: Motion Models of Ballistic and Space Targets, IEEE Transactions on Aerospace and Electronic Systems 46 (1) (2010) 96–119.

[2] Y. Li, T. Kirubarajan, Y. Bar-Shalom, M. Yeddanapudi, Trajectory and Launch Point Estimation for Ballistic Missiles from Boost Phase LOS Measurements, in: IEEE Aerospace Conference, Snowmass at Aspen, CO, USA, 1999.

[3] N. Wu, L. Chen, Y. Lei, F. Meng, Adaptive estimation algorithm of boost-phase trajectory using binary asynchronous observation, Proceedings of the Institution of Mechanical Engineers, Part G: Journal of Aerospace Engineering 230 (14) (2016) 2661–2672.

[4] L. Wu, W. Sheng, W. An, A trajectory tracking algorithm in boost phase based on mle-ckf federated filter, Journal of Computational and Theoretical Nanoscience 13 (5) (2016) 3036–3042.

[5] X. He, Y. Bi, Y. Guo, Target tracking algorithm of ballistic missile in boost phase based on ground-based radar systems, Journal of Information and Computational Science 12 (2) (2015) 855–864.

[6] A. Mukherjee, D. Mukherjee, A. Sengupta, Filter design for tracking of ballistic target missile using seeker measurements with time lag, in: 2013 International Conference on Signal Processing, Image Processing and Pattern Recognition, Coimbatore, India, 2013.

[7] C. Chen, D. Zhou, Study on a new algorithm for tracking ballistic missile in free flight phase, Advanced Materials Research 981 (2014) 743–753.

[8] G. Siouris, G. Chen, J. Wang, Tracking an Incoming Ballistic Missile Using an Extended Interval Kalman Filter, IEEE Transactions on Aerospace and Electronic Systems 33 (1) (1997) 232–240.

[9] M. Bruno, A. Pavlov, Improved Sequential Monte Carlo Filtering for Ballistic Target Tracking, IEEE Transactions on Aerospace and Electronic Systems 41 (3) (2005) 1103–1108.

[10] J. Kim, S. Vaddi, S. Menon, E. Ohlmeyer, Comparison Between Nonlinear Filtering Techniques for Spiraling Ballistic Missile State Estimation, IEEE Transactions on Aerospace and Electronic Systems 48 (3) (2012) 313–328.

[11] X. Ning, Z. Chen, X. Li, Ballistic target tracking algorithm based on improved particle filtering, in: Proc. SPIE 9675, AOPC 2015: Image Processing and Analysis, 96752B, 2015.

[12] R. Cooperman, Tactical ballistic missile tracking using the interacting multiple model algorithm, in: The Fifth International Conference on Information Fusion, Annapolis, MD, USA, 2002.

[13] W. Farrell, Tracking of a Ballistic Missile with A-Priori Information, IEEE Transactions on Aerospace and Electronic Systems 44 (2) (2008) 418–426.

[14] J. Jung, D. Hwang, The novel impact point prediction of a ballistic target with interacting multiple models, in: 13th International Conference on Control, Automation and Systems, Gwangju, Korea, 2013.

[15] H. Song, Y. Han, Comparison of space launch vehicle tracking using different types of multiple models, in: 2016 19th International Conference on Information Fusion (FUSION), Heidelberg, Germany, 2016.

[16] E. Mazor, A. Averbuch, Y. Bar-Shalom, J. Dayan, Interacting Multiple Model Methods in Target Tracking: A Survey, IEEE Transactions on Aerospace and Electronic Systems 34 (1) (1998) 103–123.

[17] T. Kirubarajan, Y. Bar-Shalom, Y. Wang, Passive Ranging of a Low Observable Ballistic Missile in a Gravitational Field, IEEE Transactions on Aerospace and Electronic Systems 37 (2) (2001) 481–494.

[18] Y. Bar-Shalom, T. Kirubarajan, X. Lin, Probabilistic Data Association Techniques for Target Tracking with Applications to Sonar,Radar and EO Sensors, IEEE Aerospace and Electronic Systems Magazine 20 (8) (2005) 37–56.

[19] H. Blom, E. Bloem, Exact Bayesian and Particle Filtering of Stochastic Hybrid Systems, IEEE Transactions on Aerospace and Electronic Systems 43 (1) (2007) 55–70.

[20] R. Mahler, Statistical multisource-multitarget information fusion, Artech House Publishers.

[21] X. Lan, H. Li, C. Li, M. Zheng, Technique of target tracking for ballistic missile, Information Technology and Intelligent Transportation Systems 454 (2016) 319–329.

[22] A. Benavoli, L. Chisci, A. Farina, Tracking of a Ballistic Missile with A-Priori Information, IEEE Transactions on Aerospace and Electronic Systems 43 (3) (2007) 1000–1016.

[23] J. Kotecha, P. Djuric, Gaussian Particle Filtering, IEEE Transactions on Signal Processing 51 (10) (2003) 2592–2601.

[24] B. Ristic, B.-T. Vo, B.-N. Vo, A. Farina, A Tutorial on Bernoulli Filters: Theory, Implementation and Applications, IEEE Transactions on Signal Processing 61 (13) (2013) 3406–3430.

[25] https://www.gov.uk/government/publications/cde-themed-competition-defence-against-airborne-threats, accessed in September, 2015.

[26] X. Li, Y. Bar-Shalom, Tracking in Clutter With Nearest Neighbor Filters: Analysis and Performance, IEEE Transactions on Aerospace and Electronic Systems 32 (3) (1996) 995–1010.

[27] R. Burden, J. Faires, Numerical analysis (5th ed.), PWS Publishing, Boston, USA.

Appendix

In the appendix, we explain the mathematical representations of BM state models during different phases in details:

Boost model

During the boost phase, the missile is affected by the gravity force, thrust force and aerodynamic drag force [22]. Besides, considering the fact that the earth rotates about the CTP axis with an angular velocity ω, the missile is also affected by two other forces: coriolis force and centripetal force. According to Newton's force law, the following basic equations hold:

$$\begin{aligned} \dot{\mathbf{p}}_t &= \mathbf{v}_t \\ \dot{\mathbf{v}}_t &= \mathbf{a}_t^{gravity} + \mathbf{a}_t^{thrust} + \mathbf{a}_t^{drag} + \mathbf{a}_t^{corriolis} + \mathbf{a}_t^{centripetal} \end{aligned} \tag{35}$$

where $\mathbf{p}_t = (p_t^x, p_t^y, p_t^z)^T$ and $\mathbf{v}_t = (v_t^x, v_t^y, v_t^z)^T$ ($(\cdot)^T$ denotes the vector transpose) represent the position and velocity in the ECEF coordinate system, respectively [1]. The vectors $\mathbf{a}_t^{gravity}$, $\mathbf{a}_t^{thrust}$, $\mathbf{a}_t^{drag}$, $\mathbf{a}_t^{corriolis}$ and $\mathbf{a}_t^{centripetal}$ represent the accelerations introduced by different types of forces as defined in [22], from which the summed acceleration of a BM along three axes of the ECEF coordinate system during the boost phase (denoted as $a_t^{x,b}$, $a_t^{y,b}$ and $a_t^{z,b}$) can be calculated as in (36).

$$\begin{aligned} a_t^{x,b} &= \frac{ng}{1-qt}\frac{v_t^x}{\sqrt{(v_t^x)^2+(v_t^y)^2+(v_t^z)^2}} - \frac{\rho(h_t)}{2\beta}v_t^x\sqrt{(v_t^x)^2+(v_t^y)^2+(v_t^z)^2} \\ &\quad - \frac{u_G}{(\sqrt{(p_t^x)^2+(p_t^y)^2+(p_t^z)^2})^3}p_t^x + (2\omega v_t^y + \omega^2 p_t^x) \\ a_t^{y,b} &= \frac{ng}{1-qt}\frac{v_t^y}{\sqrt{(v_t^x)^2+(v_t^y)^2+(v_t^z)^2}} - \frac{\rho(h_t)}{2\beta}v_t^y\sqrt{(v_t^x)^2+(v_t^y)^2+(v_t^z)^2} \\ &\quad - \frac{u_G}{(\sqrt{(p_t^x)^2+(p_t^y)^2+(p_t^z)^2})^3}p_t^y + (2\omega v_t^x + \omega^2 p_t^y) \\ a_t^{z,b} &= \frac{ng}{1-qt}\frac{v_t^z}{\sqrt{(v_t^x)^2+(v_t^y)^2+(v_t^z)^2}} - \frac{\rho(h_t)}{2\beta}v_t^z\sqrt{(v_t^x)^2+(v_t^y)^2+(v_t^z)^2} \\ &\quad - \frac{u_G}{(\sqrt{(p_t^x)^2+(p_t^y)^2+(p_t^z)^2})^3}p_t^z \end{aligned} \tag{36}$$

The parameters are defined as: $u_G = 3.99 \times 10^{14} Nm^2/kg$, $g = 9.81 ms^{-2}$ and $\omega = 7.29 \times 10^{-5} rad/s$ represent a positive constant, the gravitational acceleration and the Earth's angular speed, respectively. The parameters n, q and β represent respectively the initial thrust-to-weight ratio, normalised mass burn rate and ballistic coefficient related to a particular type of ballistic missile [22]; h_t represents the altitude of the BM at the time instance t and $\rho(\cdot)$ is the air density function defined as:

$$\rho(h_t) = \rho_0 \exp(-k \cdot h_t) \tag{37}$$

where $\rho_0 = 1.22$ and $k = 0.14 \times 10^{-3}$.

From the acceleration terms in (36) and the piecewise-constant acceleration assumption during

a short time interval T, we can obtain the evolution of the position and velocity between t and $t+T$ as:

$$\begin{aligned}
p_{t+T}^x &= p_t^x + T \cdot v_t^x + \frac{T^2}{2}(a_t^{x,b} + w_t^{x,b}) \\
p_{t+T}^y &= p_t^y + T \cdot v_t^y + \frac{T^2}{2}(a_t^{y,b} + w_t^{y,b}) \\
p_{t+T}^z &= p_t^z + T \cdot v_t^z + \frac{T^2}{2}(a_t^{z,b} + w_t^{z,b}) \\
v_{t+T}^x &= v_t^x + T \cdot (a_t^{x,b} + w_t^{x,b}) \\
v_{t+T}^y &= v_t^y + T \cdot (a_t^{y,b} + w_t^{y,b}) \\
v_{t+T}^z &= v_t^z + T \cdot (a_t^{z,b} + w_t^{z,b})
\end{aligned} \tag{38}$$

where $w_t^{x,b}$, $w_t^{y,b}$ and $w_t^{z,b}$ represent the boost phase acceleration uncertainties in three axes.

Typically, as ballistic missile parameters n, q and β in (36) are unknown, they need to be estimated. The estimated parameters can then be used in missile trajectory prediction and missile type identification. In order to estimate the initial thrust-to-weight ratio n and normalised mass burn rate q, a simple Brownian motion model is used as:

$$\begin{aligned}
n_{t+T} &= n_t + T \cdot w_n \\
q_{t+T} &= q_t + T \cdot w_q
\end{aligned} \tag{39}$$

where w_n and w_q represent the introduced parameter uncertainties.

A similar way could be used to model β. However, when the BM is at a high altitude, the value of $\frac{\rho(h_t)}{2\beta}$ in (36) will be close to zero no matter the value of β, due to the exponential decay of the term $\rho(h_t)$ with respect to the height h_t. In this case, different values of β have the same effect on the position and velocity evolution, and thus the value of β can not be estimated correctly. In order to address this issue, we adopt the same strategy for parameter modelling used in [8]. Instead of β, a parameter $\gamma_t = \frac{\rho(h)}{2\beta}$ is first modelled and calculated. And β can then be computed from γ_t. By the Euler approximation [27], the evolution of γ_t can be modelled as:

$$\gamma_{t+T} = \gamma_t + T \cdot \gamma_t' + T \cdot w_\gamma \tag{40}$$

where w_γ represents the parameter uncertainty and γ_t' represents the differentiation of γ_t with respect to the time t given as:

$$\gamma_t' = -k \cdot \gamma_t \frac{p_t^x v_t^x + p_t^y v_t^y + p_t^z v_t^z}{\sqrt{(p_t^x)^2 + (p_t^y)^2 + (p_t^z)^2}}. \tag{41}$$

By augmenting the state dynamic equation (38) with the parameter models in (39) and (40),

the complete state model for the boost phase is represented as:

$$\mathbf{x}_{t+T}^{b} = F^{b}\mathbf{x}_{t}^{b} + G^{b}\left(\begin{bmatrix} \mathbf{a}_{t}^{b} \\ \gamma_{t}' \\ 0 \\ 0 \end{bmatrix} + \mathbf{w}_{t}^{b}\right) \tag{42}$$

where

$$\begin{aligned}
\mathbf{x}_{t}^{b} &= \begin{bmatrix} p_t^x \\ p_t^y \\ p_t^z \\ v_t^x \\ v_t^y \\ v_t^z \\ \gamma_t \\ n_t \\ q_t \end{bmatrix}, \quad F^{b} = \begin{bmatrix} 1 & 0 & 0 & T & 0 & 0 & 0 & 0 & 0 \\ 0 & 1 & 0 & 0 & T & 0 & 0 & 0 & 0 \\ 0 & 0 & 1 & 0 & 0 & T & 0 & 0 & 0 \\ 0 & 0 & 0 & 1 & 0 & 0 & 0 & 0 & 0 \\ 0 & 0 & 0 & 0 & 1 & 0 & 0 & 0 & 0 \\ 0 & 0 & 0 & 0 & 0 & 1 & 0 & 0 & 0 \\ 0 & 0 & 0 & 0 & 0 & 0 & 1 & 0 & 0 \\ 0 & 0 & 0 & 0 & 0 & 0 & 0 & 1 & 0 \\ 0 & 0 & 0 & 0 & 0 & 0 & 0 & 0 & 1 \end{bmatrix} \\
G^{b} &= \begin{bmatrix} \frac{T^2}{2} & 0 & 0 & 0 & 0 & 0 \\ 0 & \frac{T^2}{2} & 0 & 0 & 0 & 0 \\ 0 & 0 & \frac{T^2}{2} & 0 & 0 & 0 \\ T & 0 & 0 & 0 & 0 & 0 \\ 0 & T & 0 & 0 & 0 & 0 \\ 0 & 0 & T & 0 & 0 & 0 \\ 0 & 0 & 0 & T & 0 & 0 \\ 0 & 0 & 0 & 0 & T & 0 \\ 0 & 0 & 0 & 0 & 0 & T \end{bmatrix} \mathbf{a}_{t}^{b} = \begin{bmatrix} a_t^{x,b} \\ a_t^{y,b} \\ a_t^{z,b} \end{bmatrix} \quad \mathbf{w}_{t}^{b} = \begin{bmatrix} w_t^{x,b} \\ w_t^{y,b} \\ w_t^{z,b} \\ w_t^{\gamma,b} \\ w_t^{n,b} \\ w_t^{q,b} \end{bmatrix}.
\end{aligned} \tag{43}$$

Coast model

During the coast phase, the BM usually follows a Keplerian orbit at a high part of or even outside the atmosphere, with the thruster ignition being off. In this case, it will not be affected by the thrust and drag forces, so the acceleration term components in three axes become:

$$\begin{aligned}
a_t^{x,c} &= -\frac{u_G}{(\sqrt{(p_t^x)^2 + (p_t^y)^2 + (p_t^z)^2})^3} p_t^x + (2\omega v_t^y + \omega^2 p_t^x) \\
a_t^{y,c} &= -\frac{u_G}{(\sqrt{(p_t^x)^2 + (p_t^y)^2 + (p_t^z)^2})^3} p_t^y + (2\omega v_t^x + \omega^2 p_t^y) \\
a_t^{z,c} &= -\frac{u_G}{(\sqrt{(p_t^x)^2 + (p_t^y)^2 + (p_t^z)^2})^3} p_t^z.
\end{aligned} \tag{44}$$

The acceleration terms do not contain any ballistic missile parameters (i.e. n, q and β) due to the

negligible thrust and drag forces. Without these BM parameters, the state model reduces to:

$$\mathbf{x}_{t+T}^{c} = F^{c}\mathbf{x}_{t}^{c} + G^{c}(\mathbf{a}_{t,c} + \mathbf{w}_{t}^{c}) \tag{45}$$

where

$$\mathbf{x}_{t}^{c} = \begin{bmatrix} p_t^x \\ p_t^y \\ p_t^z \\ v_t^x \\ v_t^y \\ v_t^z \end{bmatrix}, \quad F^{c} = \begin{bmatrix} 1 & 0 & 0 & T & 0 & 0 \\ 0 & 1 & 0 & 0 & T & 0 \\ 0 & 0 & 1 & 0 & 0 & T \\ 0 & 0 & 0 & 1 & 0 & 0 \\ 0 & 0 & 0 & 0 & 1 & 0 \\ 0 & 0 & 0 & 0 & 0 & 1 \end{bmatrix}, \quad G^{c} = \begin{bmatrix} \frac{T^2}{2} & 0 & 0 \\ 0 & \frac{T^2}{2} & 0 \\ 0 & 0 & \frac{T^2}{2} \\ T & 0 & 0 \\ 0 & T & 0 \\ 0 & 0 & T \end{bmatrix} \tag{46}$$

$$\mathbf{a}_{t}^{c} = \begin{bmatrix} a_t^{x,c} \\ a_t^{y,c} \\ a_t^{z,c} \end{bmatrix} \quad \mathbf{w}_{t}^{c} = \begin{bmatrix} w_t^{x,c} \\ w_t^{y,c} \\ w_t^{z,c} \end{bmatrix}$$

and $\mathbf{w}_t^c$ represents the coast model uncertainty.

Reentry model

At the terminal stage of the BM flight, the BM re-enters the low part of the atmosphere (i.e. troposphere and stratosphere). It is affected by the drag force again and the related acceleration terms in three axes become (47):

$$\begin{aligned} a_t^{x,r} &= -\frac{\rho(h_t)}{2\beta} v_t^x \sqrt{(v_t^x)^2 + (v_t^y)^2 + (v_t^z)^2} - \frac{u_G}{(\sqrt{(p_t^x)^2 + (p_t^y)^2 + (p_t^z)^2})^3} p_t^x + (2\omega v_t^y + \omega^2 p_t^x) \\ a_t^{y,r} &= -\frac{\rho(h_t)}{2\beta} v_t^y \sqrt{(v_t^x)^2 + (v_t^y)^2 + (v_t^z)^2} - \frac{u_G}{(\sqrt{(p_t^x)^2 + (p_t^y)^2 + (p_t^z)^2})^3} p_t^y + (2\omega v_t^x + \omega^2 p_t^y) \\ a_t^{z,r} &= -\frac{\rho(h_t)}{2\beta} v_t^z \sqrt{(v_t^x)^2 + (v_t^y)^2 + (v_t^z)^2} - \frac{u_G}{(\sqrt{(p_t^x)^2 + (p_t^y)^2 + (p_t^z)^2})^3} p_t^z. \end{aligned} \tag{47}$$

By assuming a piecewise-constant acceleration model and considering the evolution of the parameter $\gamma_t = \frac{\rho(h_t)}{2\beta}$ in (40) and (41), the state model for the reentry phase is represented as:

$$\mathbf{x}_{t+T}^{r} = F^{r}\mathbf{x}_{t}^{r} + G^{r}\left(\begin{bmatrix} \mathbf{a}_t^r \\ \gamma_t' \end{bmatrix} + \mathbf{w}_t^r\right) \tag{48}$$

where

$$\mathbf{x}_t^r = \begin{bmatrix} p_t^x \\ p_t^y \\ p_t^z \\ v_t^x \\ v_t^y \\ v_t^z \\ \gamma_t \end{bmatrix}, \quad F^r = \begin{bmatrix} 1 & 0 & 0 & T & 0 & 0 & 0 \\ 0 & 1 & 0 & 0 & T & 0 & 0 \\ 0 & 0 & 1 & 0 & 0 & T & 0 \\ 0 & 0 & 0 & 1 & 0 & 0 & 0 \\ 0 & 0 & 0 & 0 & 1 & 0 & 0 \\ 0 & 0 & 0 & 0 & 0 & 1 & 0 \\ 0 & 0 & 0 & 0 & 0 & 0 & 1 \end{bmatrix}, \quad G^r = \begin{bmatrix} \frac{T^2}{2} & 0 & 0 & 0 \\ 0 & \frac{T^2}{2} & 0 & 0 \\ 0 & 0 & \frac{T^2}{2} & 0 \\ T & 0 & 0 & 0 \\ 0 & T & 0 & 0 \\ 0 & 0 & T & 0 \\ 0 & 0 & 0 & T \end{bmatrix} \tag{49}$$

$$\mathbf{a}_t^r = \begin{bmatrix} a_t^{x,r} \\ a_t^{y,r} \\ a_t^{z,r} \end{bmatrix}, \quad \mathbf{w}_t^r = \begin{bmatrix} w_t^{x,r} \\ w_t^{y,r} \\ w_t^{z,r} \\ w_t^{\gamma,r} \end{bmatrix}.$$